ACS OMEGA

Open Access

http://pubs.acs.org/journal/acsodf

Article

Engineering Amorphous IGZO Thin-Film Transistors: The Role of Composition and Channel Thickness in Mobility-Threshold Voltage Optimization

Taehyun Kim,[§] Hyeongjun Jang,[§] Beomjin Park, Seokyeon Shin, Muhammad A. Alam, Peide D. Ye, and Changwook Jeong*

Cite This: https://doi.org/10.1021/acsomega.5c09705

Read Online

ACCESS | Metrics & More | Article Recommendations | Supporting Information

ABSTRACT: Recently, it has been shown that the mobility of amorphous InGaZnO (a-IGZO) thin-film transistors (TFTs) depends strongly on channel thickness and metal composition (In/Ga/Zn), resulting in a mobility-threshold voltage (V_{th}) trade-off. To the best of our knowledge, this work provides the first comprehensive modeling study systematically integrating density functional theory (DFT) and machine learning potential (MLP) to capture structural disorder and thickness effects on mobility-V_{th} in amorphous IGZO. We establish the existence of a universal mobility-V_{th} trade-off across diverse IGZO compositions and channel thicknesses. To unveil the origin of the universal trend, we developed a mobility model that covers the full composition and thickness of a-IGZO with composition-resolved parameters using DFT and MLP, taking into account its stochastically and structurally driven variation of the amorphous material's properties. We found that the origin of the mobility-V_{th} trade-off is the strong dependence of both mobility and V_{th} on the carrier concentration. Despite the existence of the mobility-V_{th} trade-off, as a method for designing enhancement-mode devices with high mobility, we propose increasing the Zn content to reduce the structural disorder.

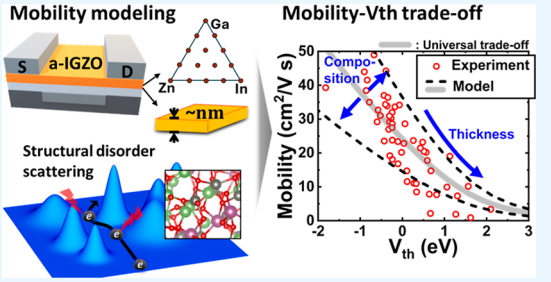

1. INTRODUCTION

In line with current advances in nanotechnology and the trajectory set by Moore's law, amorphous oxide semiconductor thin-film transistors (AOS-TFTs) have attracted significant attention because of their high electron mobility and low power consumption, positioning them as critical technologies for the next generation of nanoelectronic devices. Among the various channel material candidates, amorphous indium gallium zinc oxide (a-IGZO) has been considered as a promising channel material, thanks to its compatibility with low-temperature processing, low off-state current, and high electron mobility. Currently, many studies are evaluating various metal compositions and adjusting the channel thickness to achieve better performance in a-IGZO. However, the mobility-threshold voltage (V_{th}) trade-off makes it challenging to design enhancement-mode devices with high mobility (i.e., devices with a positive threshold voltage, $V_{th} > 0$).[1−3] Recent experimental studies have found that this trade-off persists across whole metal compositions and thicknesses from bulk to nanometer scales.

To overcome the trade-off and achieve enhancement-mode devices with high mobility, it is essential to identify the underlying physics that causes this trade-off. To date, a comprehensive mobility model incorporating thickness effects and a wide range of metal compositions in a-IGZO has not been proposed. Although the mobility model proposed by Kang et al.[4] aligns well with experimental observations, it primarily addresses crystalline IGZO structures and a limited compositional scope, without considering thickness effects. Thus, there is an evident need for a more comprehensive and systematic approach. Extending prior work, we established a model capable of predicting mobility in amorphous IGZO across a wide range of compositions and thicknesses, ultimately capable of predicting a mobility-V_{th} trade-off. Without any experimentally fitted parameters, the model relies on material parameters derived from density functional theory (DFT) simulations, in which atomic amorphous structures were generated using molecular dynamics (MD) simulation assisted with machine-learning potential (MLP). Sequentially, mobility is theoretically modeled based on Boltzmann transport theory (BTE) including electron scattering caused by **structural disorder (SD)** inherent in the amorphous structure in addition to the polar optical phonon (POP) and ionized impurity (II) scatterings.[4,5] The mobility model is further extended to

Received: September 17, 2025
Revised: November 23, 2025
Accepted: December 2, 2025

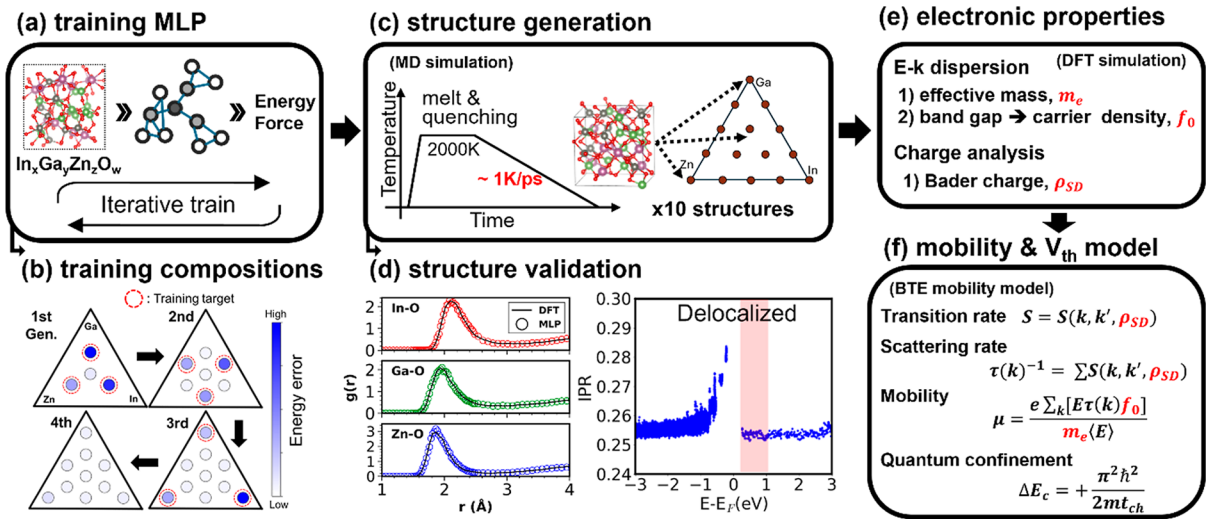

Figure 1. Schematic framework for mobility and V_{th} modeling, integrating atomistic simulations and the BTE-based scattering model across various a-IGZO compositions. (a–b) Iterative training process of MLP to span the entire composition space of a-IGZO. (c) Structure generation via MLP-interfaced MD for each composition. (d) Validation of generated structures: comparison of metal-oxygen radial distribution functions (RDF) obtained from DFT and MLP (left), and the inverse participation ratio of the generated 1:1:1 a-IGZO structure (right). RDFs for other compositions are presented in Figure S2. (e) Calculation of electronic parameters (highlighted in red) from DFT simulation, used for the mobility model. (f) Construction of a BTE mobility model incorporating quantum confinement effects for the V_{th} model.

capture the effect of variation in scattering, attributed to the variety of amorphous configurations. Meanwhile, the V_{th} is modeled to embed the quantum confinement (QC) effect to describe a **few-nanometer thin-film transistor** as well. To sum up, the integrated framework is proposed to bridge materials on the atomic scale to device-level modeling, benefiting from recent advancements in computational material sciences. This leads to the understanding of the origin of the mobility-V_{th} trade-off in IGZO thin-film transistors.

2. THEORY AND COMPUTATIONAL DETAILS

The procedure of material simulations and theoretical modeling, illustrated in Figure 1, consists of three steps: (a–d) generation of atomistic a-IGZO structures, (e) extraction of material parameters using DFT, and (f) modeling mobility and V_{th}. The first two steps include atomistic simulations carried out to acquire reliable material parameters without experimental data. In the last step, the extracted parameters are fed to the mobility and V_{th} model.

2.1. Generation of Amorphous Structures. Amorphous structures in atomistic simulations allow for the exploration of various compositions while capturing the SD scattering and stochastic variations inherent to disordered materials. To generate thermodynamically plausible amorphous configurations, melt-quenching MD simulations are employed. In addition, machine-learning potential (MLP)[6] is primarily developed to enable efficient execution of multiple MD simulations with accuracy comparable to that of DFT,[7] thereby reproducing SD in a reliable manner (Figure 1a). To span the entire compositional space—from the 1:1:1 point to boundary regions—MLP training iteratively incorporates structures exhibiting high prediction errors, ensuring robust coverage of structural variability (Figure 1a,b). For each composition, ten structures were generated by performing melt-quenching MD, and the generated structures were analyzed to ensure a reliable representation of structural variability and statistical robustness (Figure 1c). All DFT simulations were performed using the QuantumATK software, version V-2023.09.[8] In Figure 1d, the generated structures are evaluated in terms of their agreement with DFT simulations using two metrics: the metal-oxygen coordination number, which reflects the structural validity of the amorphous phase, and the inverse participation ratio, which characterizes the delocalization of conduction band edge,[9] and thus the electronic validity.

2.2. Electronic Parameters of IGZO with Various Compositions. In Figure 1e, the effective masses, SD scattering center densities (ρ_{SD}), and band gaps are obtained from DFT calculations of the generated structures. Carrier concentrations are determined based on the calculated band gaps and the experimentally reported Fermi level (E_F) position. The relative position of the Fermi level with respect to the conduction band edge was adjusted such that the carrier concentration of the 1:1:1 composition matches the experimental value reported in ref 10. The Fermi-level positions of other compositions were subsequently shifted by half of the band gap difference ($\sim 1/2\Delta E_{gap}$) based on the DFT-calculated band gap data, and the corresponding n_e values were derived using a parabolic band model. Since E_F has been reported to remain nearly constant at the charge neutrality level throughout the composition,[11−13] carrier concentrations are calculated based on the relative position of the conduction band edge to E_F. The ρ_{SD} is derived from variations in the charge distribution induced by diverse local bonding environments of the amorphous configuration, which is quantified through Bader charge analysis within the DFT framework. Additional details regarding the simulation settings and procedures are provided in Supporting Information S1.

2.3. Mobility and V_{th} Modeling of AOS. The mobility model is based on the solution of the Boltzmann transport equation (BTE) with relaxation time approximation including polar optical phonon (POP), ionized impurity (II), and mainly SD scattering[4,5] (Supporting Information S2). The implemented dependence of mobility on carrier concentration and temperature shows good agreement with experimental data (Supporting Information S3). An increase in carrier concentration and temperature leads to enhanced mobility, and this

https://doi.org/10.1021/acsomega.5c09705
ACS Omega XXXX, XXX, XXX−XXX

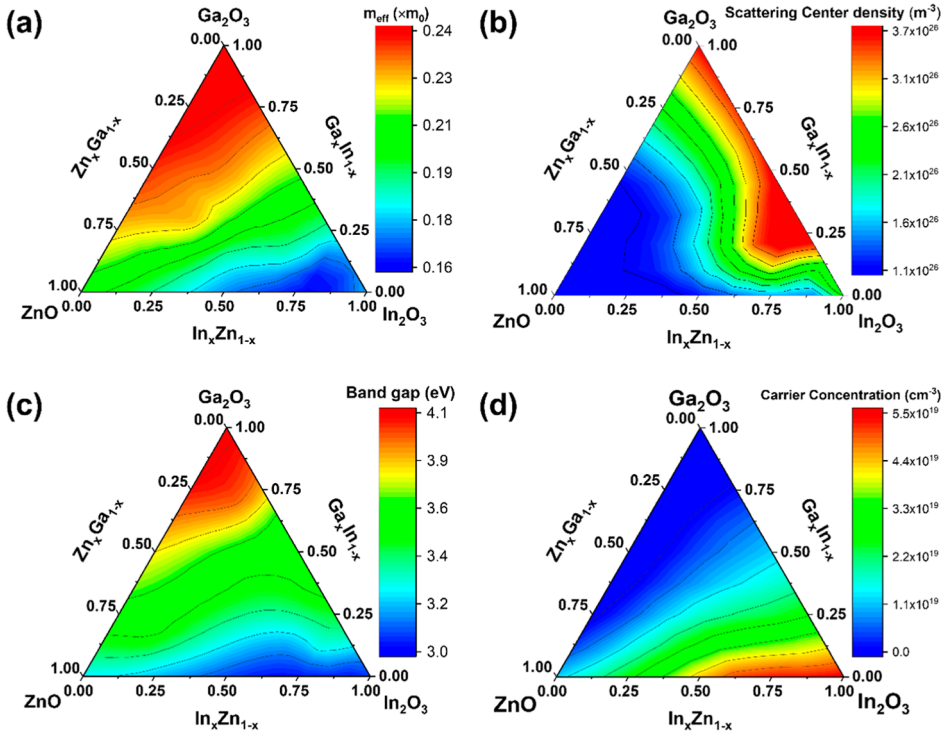

Figure 2. A ternary map of (a) effective mass, (b) ρ_{SD}, (c) band gap, and (d) carrier concentration of a-IGZOs. The data presented on the ternary maps represent averages over ten different a-IGZO for each composition. The carrier concentration is calculated based on the band gap values, as detailed in the main text.

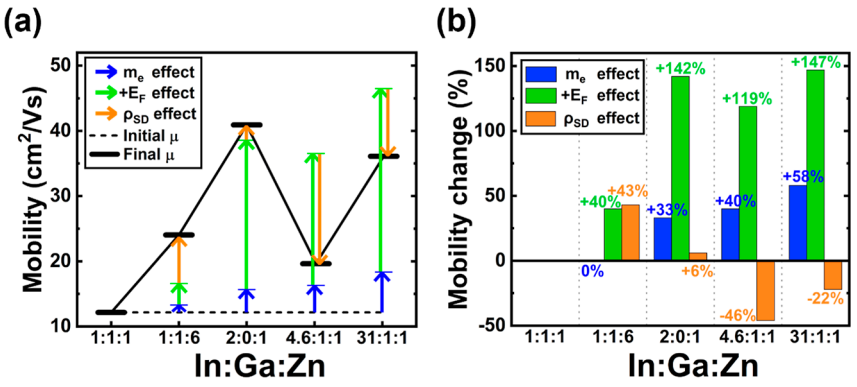

Figure 3. Three factors (E_F, ρ_{SD}, and m^*) affecting mobility and their extent for various compositions. (a) The mobility value of compositions, contributed by composition-dependent factors, and (b) the corresponding mobility changes. E_F is the most dominant factor, but ρ_{SD} also has an impact on compositions containing Zn. The effect of the dielectric constant is negligible, which is not shown here.

dependence on carrier concentration becomes more pronounced at low temperatures (Figure S4c). This behavior indicates that high-energy electrons are able to overcome the hopping barriers, where materials with higher carrier concentrations and temperatures tend to contain a larger population of such energetic carriers. Accordingly, the energetic profile of potential barriers is a key determinant in mobility modeling. In this work, two distinct origins of energy barriers are *implicitly* considered in this methodology: (1) electrostatic potential variations induced by structural disorder (SD), which lead to fluctuations in conduction band states; and (2) the compositional contribution arising from the specific metal content. Furthermore, the carrier concentration remains a critical factor, particularly in the thin-film transistor, where the quantum confinement effect in thin materials widens the band gap considered in the V_{th} model (Supporting Information S4 and S5). To sum up, the effects of SD, composition, and the carrier concentration−thickness relation are comprehensively integrated into the mobility model.

The hopping barrier for electrons caused by SD in a-IGZO is quantified by analyzing the charge distribution for all atoms within each structure, as obtained from DFT through Bader charge analysis (Supporting Information, S6 and S7). Variations in Bader charge among identical cations are interpreted as effective charged scattering centers, here termed SD scattering centers (ρ_{SD}), corresponding to the local electrostatic potential fluctuations. In this regard, using the Coulomb scattering formula, SD scattering is included in the mobility model. Since SD scattering is anisotropic, the scattering rate is obtained by considering the scattering angle. Overall, the model captures both the carrier concentration and SD scattering effects. High electron mobility

https://doi.org/10.1021/acsomega.5c09705
ACS Omega XXXX, XXX, XXX−XXX

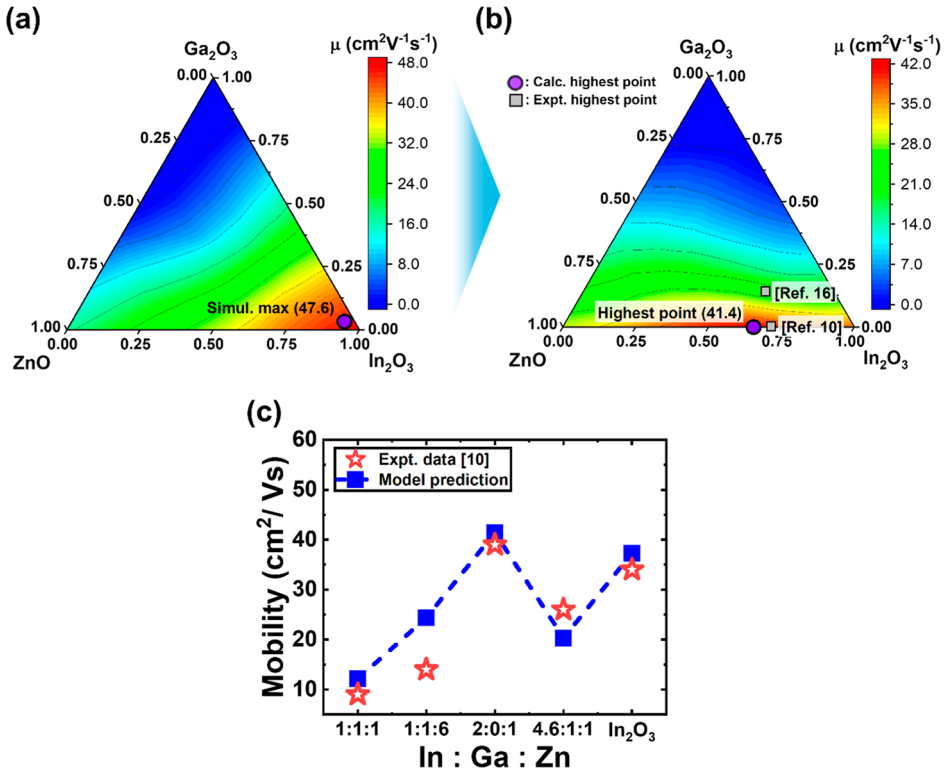

Figure 4. Ternary maps of predicted mobility incorporating composition-dependent m_e and E_F values: (a) without ρ_{SD} dependence and (b) ρ_{SD} dependence included. (c) Comparison of the mobility values of five different compositions, In/Ga/Zn = 1:1:1, 1:1:6, 2:0:1, 4.6:1:1, and 1:0:0, between experimental measurements and model predictions. The composition of maximum mobility changes from In-rich to $In_2Zn_1O_4$ with 41.4 $cm^2/V{\cdot}s$.

is achieved when a larger population of high-energy electrons is present and the hopping barriers are low; otherwise, the mobility is significantly reduced.

3. RESULTS AND DISCUSSION

3.1. Maximum Mobility across the Composition. In Figure 2a and c, the In-rich region exhibits a low band gap, leading to high carrier concentrations and small effective mass. Compositions composed of cations with a large principal quantum number, with substantial overlap between the *ns* orbitals of nearest-neighboring cations, enhance conduction band dispersion. As a result, the band gap narrows and the effective mass decreases.[14] These trends have been reported experimentally and are consistent with our calculated band gap and effective mass. In Figure 2d, the In-rich area shows the highest carrier concentration, followed by the Zn-rich area, while the Ga-rich area shows the lowest carrier concentration. This trend is consistent with experimental observations.[10,15,16] In Figure 2b, the Zn-rich area has a lower ρ_{SD} than the In-rich or Ga-rich areas. Ga and In exhibit mixed coordination environments, forming both GaO_4/GaO_6 and InO_5/InO_6 units, whereas Zn predominantly forms ZnO_4 with a constant Zn−O bond length of approximately 1.97 Å. Therefore, when SD occurs, Zn exhibits less variation in the extent of electron transfer to oxygen compared with Ga and In. Consequently, fewer ρ_{SD} are formed in Zn-containing compositions in a-IGZO.

In Figure 3, an ablation study is performed to assess the contribution of three parameters to the mobility of a-IGZO, by comparing the calculated mobility values with those of the 1:1:1 (=In/Ga/Zn) composition. In Figure 3a, the ablation study confirms that the composition-dependent parameters—such as effective mass (m_e), E_F, and ρ_{SD}—significantly impact the mobility, as evidenced by deviations from the mobility values of the 1:1:1 composition. Figure 3b shows that, across most compositions, the key determinants of mobility are m_e and carrier concentration in terms of E_F, whereas the influence of ρ_{SD} remains significant for 1:1:6 and 4.6:1:1 compositions by ∼45%. The dielectric constants of IGZO, In_2O_3, ZnO, and Ga_2O_3 are 9.06, 8.90, 8.60, and 9.93, respectively, and do not vary significantly with metal composition.[17,18]

Figure 4a presents the mobility across the ternary compositions, in which the mobility is calculated with composition-dependent m_e and E_F in the absence of SD scattering. It shows that the composition with high carrier concentration, particularly with the indium-rich composition, performs the highest mobility. Nevertheless, as shown in the ablation study, ρ_{SD} remains a major factor influencing mobility, particularly in Zn-rich compositions. In Figure 4b, mobility is recalculated with the additional inclusion of ρ_{SD}, resulting in a slight shift of the maximum mobility composition from the In-rich side toward the Zn-rich side—remarkably consistent with experimental observations.[10,19] Unlike In or Ga, Zn has a coordination number of 4, which leads to relatively fewer variations in bonding characteristics and thereby Bader charge values within the amorphous structure. This behavior is consistent with an analysis using the Maxwell rule and topological constraint theory, which indicates that Zn forms a less constrained amorphous network compared with In or Ga. Additional details can be found in Supporting Information S8. Consequently, at the optimal 2:0:1 (In/Ga/Zn) composition identified by our calculations, favorable transport

https://doi.org/10.1021/acsomega.5c09705
ACS Omega XXXX, XXX, XXX−XXX

conditions—high carrier concentration and low effective mass—are predominantly provided by the high In content. Simultaneously, the increased Zn content contributes to a reduction in ρ_{SD}, thereby leading to the highest overall mobility. As shown in Figure 4c, our mobility model accurately reproduces the experimental mobility values for the main metal compositions of a-IGZO.

3.2. Universal Mobility-V_{th} Trade-off with Nanoscale Channel Thickness. Furthermore, the proposed model is extended from the bulk to the nanometer-thickness regime, which is primarily responsible for the emergence of universal mobility-V_{th} trade-off behavior. Variations in IGZO channel thickness significantly influence key device performance such as mobility and V_{th}.[1−3] This effect is particularly pronounced as the thickness is reduced to sub-10 nm scales. At the nanoscale, a reduced thickness induces quantum confinement, which widens the band gap and shifts the E_F downward relative to the conduction band minimum. As a result, the carrier concentration in the channel decreases, leading to a positive shift in the V_{th}. Simultaneously, the reduction in the number of high-energy electrons—responsible for overcoming potential barriers—leads to an increase in the effective barrier height, thereby decreasing the mobility (Figure 5a). Therefore, both

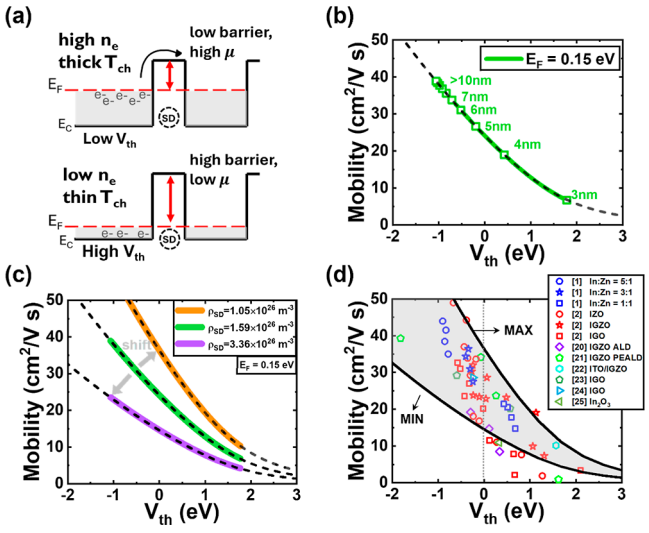

Figure 5. (a) An illustration of the mobility change caused by the reduction of thickness and carrier concentration that makes the barrier relatively high. (b) Owing to the relation of mobility and E_F, a mobility and V_{th} trade-off arises, marked by the black dashed line. In the absence of any compositional change, the mobility values consistently lie on the curve, even with varying thickness and carrier concentration (or E_F). (c) For different values of ρ_{SD}, the curves split: an orange-colored line indicates Zn-rich composition with the lowest ρ_{SD}, while the purple corresponds to the In-rich composition with the highest ρ_{SD}. (d) Comparison between the experimental mobility-V_{th} values of TFTs[1,2,20−25] and the predicted values.

mobility and V_{th} in a-IGZO are strongly influenced by the metal composition as well as channel thickness. As shown in Figure 5b, a decrease in thickness leads to a positive shift in the V_{th} and a reduction in mobility. Notably, the data points in the mobility-V_{th} plot consistently align along a **universal mobility-V_{th} trade-off line** (the black dashed line), regardless of the Fermi level position in the bulk or the degree of thickness scaling. This behavior originates from the dominant influence of carrier concentration on both V_{th} and mobility. In Figure 5c, the green line moves upward and downward depending on whether ρ_{SD} decreases or increases, respectively. The orange line corresponds to the Zn-rich region, where ρ_{SD} is minimized, while the purple line represents the In-rich region, where it reaches a maximum. In Figure 5d, the gray region is bound by the maximum and minimum trade-off curves derived in Figure 5c, in which the mobility-V_{th} characteristics of a-IGZO are expected to lie. Most of the experimental data from AOS TFTs are found to be bound within this region.[1,2,20−25] The influence of ρ_{SD} is unambiguously observed in the experimental data from ref 1, as represented by the blue markers. As the indium content increases, both a negative shift in V_{th} and an enhancement in mobility are observed, attributed to the increase in the carrier concentration. In contrast, with increasing Zn content, the data points approach the upper trade-off boundary, reflecting the reduction in SD.

To succinctly represent this trade-off, we propose an analytical expression approximated from our numerical mobility model. When ρ_{SD} is sufficiently high, the numerical formula can be approximated analytically (see Figure 6a),

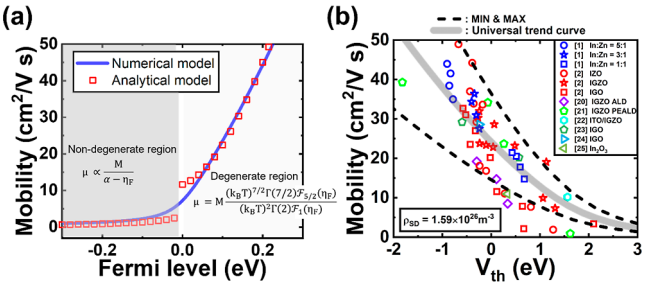

Figure 6. (a) The analytical model is derived in the nondegenerate region and the degenerate region using approximations. This simple equation clarifies the mobility dependence on E_F, where $\eta_F = (E_F - E_C) / (k_BT)$ and $\mathcal{F}_i$ is the Fermi Dirac integral. The analytical model agrees well with the numerical model in the energy range where electrons can exist at room temperature. The analytical model also exhibits temperature dependency as well as E_F dependency. The coefficients M and α are presented in Supporting Information S9. (b) The mobility values, calculated by the analytical model, are plotted to compare with experimental data, at $\rho_{SD} = 1.59 \times 10^{26}$ m^{-3}. The curve is matched well with the AOS TFT experiment data. The legend is the same as in Figure 5d.

revealing a proportionality of mobility and E_F and an explicit relationship between mobility and V_{th}. The full derivation and approximation details are provided in Supporting Information S9. In Figure 6b, the analytical model agrees well with the various experimental mobility-V_{th} data points, as well.

In terms of the model's limitations, it incorporates neither the influence of oxygen vacancy concentration, which can vary significantly depending on processing conditions, nor the corresponding dependence of carrier concentration and ρ_{SD}. Moreover, a noticeable deviation exists between the model-predicted and experimental mobility values, with a root-mean-square error (RMSE) ranging from approximately 7 to 15 cm^2/V·s (see Figure S8). Furthermore, as reported in recent studies,[26,27] extrinsic factors such as the incorporation of Hf dopants and the formation of heterostructures to achieve simultaneous mobility enhancement and stability improvement remain beyond the predictive scope of the present model. In addition, the composition-dependent device design strategies proposed herein do not consider stability effects, particularly in

https://doi.org/10.1021/acsomega.5c09705
ACS Omega XXXX, XXX, XXX−XXX

Ga-free InZnO compositions, where oxygen vacancies can generate trap states and degrade the electrical stability.

4. CONCLUSION

To summarize, we established the framework to analyze AOSs TFTs by applying MLP and DFT to the structural disorder scattering mobility modeling. Considering the Bader charge difference in the a-IGZO structure, we accurately reproduced the trend of mobility in the entire composition of bulk a-IGZO. Also, we advanced our model for a thin-channel device with the QC effect, which shows agreement with the experimental results as well. Additionally, we revealed a universal mobility-V_{th} trend spanning from the nanometer scale to bulk IGZO channels, validating it through both analytical derivations and experimental results.

To design enhancement-mode devices with high mobility, strategies to modify the mobility-V_{th} trade-off must be developed. Due to the presence of hopping barriers in the conduction band, overcoming this trade-off is challenging, as mobility is strongly governed by carrier concentration. However, the trade-off curve can be shifted by appropriately tuning the Zn content in the metal composition to reduce the ρ_{SD}. Significantly, these findings highlight that not only increasing the carrier concentration—whether through thickness adjustment, as proposed here, or via doping methods such as oxygen vacancy formation—but also reducing ρ_{SD} is essential for attaining both high mobility and enhancement-mode operation.

■ ASSOCIATED CONTENT

Supporting Information

The Supporting Information is available free of charge at https://pubs.acs.org/doi/10.1021/acsomega.5c09705.

(S1) DFT and MLP−MD simulation settings and training; (S2) scattering mechanisms and mobility calculations; (S3) scattering rates and mobility dependence on carrier concentration and temperature; (S4) threshold-voltage modeling as a function of channel thickness including QC; (S5) QC effects in ultrathin oxide semiconductors; (S6) definition and extraction of structural-disorder (SD) scattering center density from Bader charge; (S7) sensitivity analysis of Bader charge calculations; (S8) Maxwell-rule and topological-constraint-theory analysis of SD reduction by Zn incorporation; and (S9) derivation of an analytical mobility equation from the numerical BTE solution (PDF)

■ AUTHOR INFORMATION

Corresponding Author

Changwook Jeong − *Graduate School of Semiconductor Materials and Devices Engineering, Ulsan National Institute of Science and Technology, Ulsan 44919, Republic of Korea;* orcid.org/0000-0003-3962-7153; Phone: +82-(0)52-217-3211; Email: changwook.jeong@unist.ac.kr

Authors

Taehyun Kim − *Graduate School of Semiconductor Materials and Devices Engineering, Ulsan National Institute of Science and Technology, Ulsan 44919, Republic of Korea;* orcid.org/0009-0009-0414-1226

Hyeongjun Jang − *Graduate School of Semiconductor Materials and Devices Engineering, Ulsan National Institute of Science and Technology, Ulsan 44919, Republic of Korea;* orcid.org/0009-0003-1455-7395

Beomjin Park − *Graduate School of Semiconductor Materials and Devices Engineering, Ulsan National Institute of Science and Technology, Ulsan 44919, Republic of Korea*

Seokyeon Shin − *Graduate School of Semiconductor Materials and Devices Engineering, Ulsan National Institute of Science and Technology, Ulsan 44919, Republic of Korea*

Muhammad A. Alam − *Elmore Family School of Electrical and Computer Engineering, Purdue University, West Lafayette, Indiana 47907, United States;* orcid.org/0000-0001-8775-6043

Peide D. Ye − *Elmore Family School of Electrical and Computer Engineering, Purdue University, West Lafayette, Indiana 47907, United States;* orcid.org/0000-0001-8466-9745

Complete contact information is available at: https://pubs.acs.org/10.1021/acsomega.5c09705

Author Contributions

[§]T.K. and H.J. contributed equally to this work. The manuscript was written through contributions of all authors. All authors have given approval to the final version of the manuscript.

Notes

The authors declare no competing financial interest.

■ ACKNOWLEDGMENTS

This work was supported by the Nano & Material Technology Development Program through the National Research Foundation of Korea, funded by the Ministry of Science and ICT (2710089547 and RS-2024-00458251). Additional support was provided by the Technology Innovation Program (RS-2023-00231956) and by a Korea Institute for Advancement of Technology (KIAT) grant (P0023703), both funded by the Ministry of Trade, Industry and Energy (MOTIE, Korea). The authors also acknowledge financial support from Samsung Electronics.

■ ABBREVIATIONS

TFT, thin-film transistor; a-IGZO, amorphous InGaZnO; DFT, density functional theory; MLP, machine learning potential; BTE, Boltzmann transport equation; QC, quantum confinement; POP, polar optical phonon; II, ionized impurity; SD, structural disorder.

■ REFERENCES

(1) Zheng, D.; Charnas, A.; Anderson, J.; Dou, H.; Hu, Z.; Lin, Z.; Zhang, Z.; Zhang, J.; Liao, P.-Y.; Si, M.; Wang, H.; Weinstein, D.; Ye, P. D. First Demonstration of BEOL-Compatible Ultrathin Atomic Layer-Deposited InZnO Transistors with GHz Operation and Record High Bias-Stress Stability. In *2022 International Electron Devices Meeting (IEDM)*; IEEE, 2022; pp 431−434.

(2) Hikake, K.; Huang, X.; Kim, S.; Sakai, K.; Li, Z.; Mizutani, T.; Saraya, T.; Hiramoto, T.; Takahashi, T.; Uenuma, M.; Uraoka, U.; Kobayashi, M. Scaling Potential of Nanosheet Oxide Semiconductor FETs for Monolithic 3D Integration−ALD Material Engineering, High-Field Transport, Statistical Variability. In *2024 IEEE Symposium on VLSI Technology and Circuits (VLSI Technology and Circuits)*; IEEE, 2024; pp 1−2.In:

(3) Ha, D.; Lee, W.; Cho, M. H.; Terai, M.; Yoo, S.-W.; Kim, H.; Lee, Y.; Uhm, S.; Ryu, M.; Sung, C.; Song, Y.; Lee, K.; Park, S. W.; Lee, K.-S.; Tak, Y. S.; Hwang, E.; Chae, J.; Im, C.; Byeon, S.; Hong,

M.; Sim, K.; Jung, W. J.; Ryu, H.; Hong, M. J.; Park, S.; Park, J.; Choi, Y.; Lee, S.; Woo, G.; Lee, J.; Kim, D. S.; Kuh, B. J.; Shin, Y. G.; Song, J. Highly Manufacturable, Cost-Effective, and Monolithically Stackable $4F^2$ Single-Gated IGZO Vertical Channel Transistor (VCT) for sub-10nm DRAM. In *2023 International Electron Devices Meeting (IEDM)*; IEEE, 2023; pp 1−4.

(4) Kang, Y.; Cho, Y.; Han, S. Cation disorder as the major electron scattering source in crystalline InGaZnO. *Appl. Phys. Lett.* **2013**, *102*, 152104.

(5) Lundstrom, M. *Fundamentals of Carrier Transport*, 2nd ed ed.; Cambridge Univ. Press: Cambridge, U.K., 2000.

(6) Batzner, S.; Musaelian, A.; Sun, L.; Geiger, M.; Mailoa, J. P.; Kornbluth, M.; Molinari, N.; Smidt, T. E.; Kozinsky, B. E (3)-equivariant graph neural networks for data-efficient and accurate interatomic potentials. *Nat. Commun.* **2022**, *13* (1), 2453.

(7) Hong, C.; Choi, J.; Jeong, W.; Kang, S.; Ju, S.; Lee, K.; Jung, J.; Youn, Y.; Han, S. Training machine-learning potentials for crystal structure prediction using disordered structures. *Phys. Rev. B* **2020**, *102* (22), 224104.

(8) Smidstrup, S.; Markussen, T.; Vancraeyveld, P.; Wellendorff, J.; Schneider, J.; Gunst, T.; Verstichel, B.; Stradi, D.; Khomyakov, P. A.; Vej-Hansen, U. G.; Lee, M.-E.; Chill, S. T.; Rasmussen, F.; Penazzi, G.; Corsetti, F.; Ojanperä, A.; Jensen, K.; Palsgaard, M. L. N.; et al. QuantumATK: an integrated platform of electronic and atomic-scale modelling tools. *J. Phys.: Condens. Matter* **2020**, *32* (1), 015901.

(9) De Meux, A. D. J.; Pourtois, G.; Genoe, J.; Heremans, P. Origin of the apparent delocalization of the conduction band in a high-mobility amorphous semiconductor. *J. Phys.: Condens. Matter* **2017**, *29* (25), 255702.

(10) Kamiya, T.; Hosono, H. Material characteristics and applications of transparent amorphous oxide semiconductors. *NPG Asia Mater.* **2010**, *2* (1), 15−22.

(11) Swallow, J. E. N.; Varley, J. B.; Jones, L. A. H.; Gibbon, J. T.; Piper, L. F. J.; Dhanak, V. R.; Veal, T. D. Transition from electron accumulation to depletion at β-Ga2O3 surfaces: The role of hydrogen and the charge neutrality level. *APL Mater.* **2019**, *7*, 022528.

(12) Van De Walle, C. G.; Neugebauer, J. Universal alignment of hydrogen levels in semiconductors, insulators and solutions. *Nature* **2003**, *423* (6940), 626−628.

(13) Walsh, A.; Da Silva, J. L. F.; Wei, S.-H. Multi-component transparent conducting oxides: progress in materials modelling. *J. Phys.: Condens. Matter* **2011**, *23* (33), 334210.

(14) Kim, J.; Bang, J.; Nakamura, N.; Hosono, H. Ultra-wide bandgap amorphous oxide semiconductors for NBIS-free thin-film transistors. *APL Mater.* **2019**, *7*, 022501.

(15) Sheng, J.; Hong, T.; Lee, H.; Kim, K.; Sasase, M.; Kim, J.; Hosono, H.; Park, J.-S. Amorphous IGZO TFT with High Mobility of ∼ 70 $cm^2/(V\ s)$ via Vertical Dimension Control Using PEALD. *ACS Appl. Mater. Interfaces* **2019**, *11* (43), 40300−40309.

(16) Kamiya, T.; Nomura, K.; Hosono, H. Electronic Structures Above Mobility Edges in Crystalline and Amorphous In-Ga-Zn-O: Percolation Conduction Examined by Analytical Model. *J. Display Technol.* **2009**, *5* (12), 462−467.

(17) Upadhyay, M.; Elbahri, M. B.; Mezhoud, M.; Germanicus, R. C.; Luders, U. Thickness dependence of dielectric properties in sub-nanometric Al_2O_3/ZnO laminates. *Solid-State Electron.* **2021**, *186*, 108070.

(18) Fiedler, A.; Schewski, R.; Galazka, Z.; Irmscher, K. Static dielectric constant of β-Ga2O3 perpendicular to the principal planes (100), (010), and (001). *ECS J. Solid State Sci. Technol.* **2019**, *8* (7), Q3083.

(19) Hong, T.; Kim, Y.-S.; Choi, S.-H.; Lim, J. H.; Park, J.-S. Exploration of Chemical Composition of In−Ga−Zn−O System via PEALD Technique for Optimal Physical and Electrical Properties. *Adv. Electron. Mater.* **2023**, *9* (4), 2201208.

(20) Zhang, J.; Lin, Z.; Zhang, Z.; Xu, K.; Dou, H.; Yang, B.; Charnas, A.; Zheng, D.; Zhang, X.; Wang, H.; Ye, P. D. Back-End-of-Line-Compatible Scaled InGaZnO Transistors by Atomic Layer Deposition. *IEEE Trans. Electron Devices* **2023**, *70*, 6651−6657.

(21) Jeong, S. G.; Jeong, H. J.; Park, J. S. Low Subthreshold Swing and High Performance of Ultrathin PEALD InGaZnO Thin-Film Transistors. *IEEE Trans. Electron Devices* **2021**, *68* (4), 1670−1675.

(22) Park, C.-Y.; Jeon, S.-P.; Park, J. B.; Park, H.-B.; Kim, D.-H.; Yang, S. H.; Kim, G.; Jo, J.-W.; Oh, M. S.; Kim, M.; Kim, Y.-H.; Park, S. K. High-performance ITO/a-IGZO heterostructure TFTs enabled by thickness-dependent carrier concentration and band alignment manipulation. *Ceram. Int.* **2023**, *49* (4), 5905−5914.

(23) Zhang, J.; Zhang, Z.; Dou, H.; Lin, Z.; Xu, K.; Yang, W.; Zhang, X.; Wang, H.; Ye, P. D. Fluorine Anion-Doped Ultra-Thin InGaO Transistors Overcoming Mobility-Stability Trade-off. In *2023 International Electron Devices Meeting (IEDM)*; IEEE, 2023; pp 1−4.

(24) Zhang, J.; Zheng, D.; Zhang, Z.; Charnas, A.; Lin, Z.; Ye, P. D. Ultrathin InGaO Thin Film Transistors by Atomic Layer Deposition. *IEEE Electron Device Lett.* **2023**, *44* (2), 273−276.

(25) Si, M.; Hu, Y.; Lin, Z.; Sun, X.; Charnas, A.; Zheng, D.; Lyu, X.; Wang, H.; Cho, K.; Ye, P. D. Why In_2O_3 Can Make 0.7 nm Atomic Layer Thin Transistors. *Nano Lett.* **2021**, *21* (1), 500−506.

(26) Kim, Y. S.; Kim, H. W.; Hwang, T.; Ahn, J.; Cho, S. B.; Park, J. S. Ultra-High Mobility Atomically-Ordered InGaZnO Transistors through Atomic Layer Deposition. *Adv. Electron. Mater.* **2025**, *11* (15), No. e00137.

(27) Kim, H. G.; Lee, H. J.; Lee, K. M.; Kim, T. G. Improved Mobility and Bias Stability of Hf-Doped IGZO/IZO/Hf-Doped IGZO Thin-Film Transistor. *J. Alloys Compd.* **2024**, *981*, 173587.

https://doi.org/10.1021/acsomega.5c09705
ACS Omega XXXX, XXX, XXX−XXX